FREE FLIGHT DETERMINATION OF BOUNDARY LAYER TRANSITION ON SMALL SCALE CONES IN THE PRESENCE OF SURFACE ABLATION (Unclassified)

by Max E. Wilkins and Gary T. Chapman

Ames Research Center, NASA, Moffett Field, Calif. 94035

INTRODUCTION

To assess the possibility of achieving extensive laminar flow on conical vehicles during hyperbolic entry, the Ames Research Center has had an ongoing program to study boundary-layer transition on ablating cones. Boundary layer transition results are presented here from ballistic range experiments with models that ablated at dimensionless mass transfer rates comparable to those expected for full scale flight at speeds up to 17 km/sec. Previous results of this study have been published in references 1-4. These early data consisted mainly of measurements of the total ablated mass and detailed studies of surface features. The measurements of mass loss were compared with the mass that should have been removed by either fully laminar or fully turbulent flow. The data all fell between these extremes and showed a reasonable progression toward the turbulent theory as the area of the model covered with clearly discernible, roughly triangular regions of increased mass removal (turbulence wedges) increased. While this correlation seemed to give a reasonable indication of the nature of the boundary-layer flow during ablation, several recovered Delrin models (which were launched at more than 5 km/sec) exhibited no perceptible turbulence wedges, but inexplicably lost more mass than predicted by laminar theory (refs. 2 and 4).

Subsequent to the publication of reference 4, it was found possible to measure the surface recession and hence more accurately identify regions of laminar, transitional, and turbulent flow along generators of the recovered cones. Some preliminary results using this technique are described in reference 1. Since then this method of interpreting data has been improved and is used extensively in the present paper.

(NASA-TM-X-68867) FREE FLIGHT DETERMINATION OF BOUNDARY LAYER TRANSITION ON SMALL SCALE CONES IN THE PRESENCE OF SURFACE ABLATION M.E. Wilkins, et al (NASA) 3 Aug. 1972 24 p CSCL 20D G3/12

N73-12293

Unclas 48967

FACILITY, MODELS, AND EXPERIMENTAL TECHNIQUE

The models were launched in free flight in air at static pressures from 0.5 to 4 atm in the Ames Pressurized Ballistic Range. Launch velocities ranged from 2 to 6 km/sec. Model cone half-angles were 30° and 50° with base diameters of 1 and 1.2 cm, respectively. The 30° cones were launched enclosed in a sabot, whereas the 50° cones were launched as cone cylinders as will be discussed later. At these velocities and free-stream pressures the models initially experience high convective heating rates and hence high ablation rates; however, because of low model density and high drag, they decelerate rapidly to low subsonic speeds after about 30 m of flight. An open cylindrical "catcher" tunnel made of aluminum and aligned with the flight path is used to capture the models essentially undamaged. (The purpose of the tunnel is to prevent the models from veering off course and damaging themselves by striking equipment within the range.)

The models were homogeneous and made of plastics strong enough to withstand the extreme launch accelerations in the light-gas-gun launch tube. The plastic, Delrin, was chiefly used although some data for Lexan and cellulose nitrate were obtained. Efforts to launch and recover Teflon models were not successful.

The surface finish on most of the 30° conical surfaces was controlled by polishing with 3/0 metallographic polishing paper. This produced a finish in the 0 to 1 micron range that proved to be much finer than required, since ablation removes material to a much greater depth. A good machine finish was found to be adequate. Some 30° conical models that had good machine finishes were launched. These gave results similar to the polished models so all of the 50° conical models were machine finished.

Most of the models launched were prepared with pointed tips. However, for a few of the 30° half-angle Delrin cones the nose was rounded prior to launch with nose radius to base radius ratios up to 9%. The nose rounding was done to determine if it had any effect on transition Reynolds number.

Analysis of Recovered Bodies

The mass loss data for the 30° cones were obtained simply by weighing the model before launch and after recovery. However, the 50° cones were flown as a cone cylinder (see fig. 1) where the model consisted of a cone with a cylindrical afterbody. This

afterbody was press fitted to the cylinder that accompanied the cone throughout the flight. After recovery, the outer cylinder was removed from the cone so that the mass loss of the conical surface could be measured. The initial mass, m_o, used to normalize the mass loss data for the 50° cones was computed for the cone itself. It does not include the weight of the cylindrical afterbody.

In addition to weighing the models to determine mass loss, enlarged profile pictures (cf. fig. 2) were utilized to determine the local surface recession. The figure shows example profiles obtained for both the 30° and 50° cones. The outer profile was taken before launch, the inner one after recovery. Between one and six profile pictures were taken before launch and as many as required after recovery. The recession, Δr, is determined from the superimposed profiles and is measured normal to the cone axis. Small errors in aligning the profile pictures can significantly affect the accuracy of the Δr measurements; rotation of one image with respect to the other and failure to align the profiles either laterally or axially. With the aid of a pedestal providing an axis reference at the model base, the errors have been greatly reduced. Lateral errors are further reduced by averaging several values of Δr around the cone at the same axial position. Since some rays may represent surface areas that experienced laminar flow and others turbulent flow, this averaging process tends to make interpretation more difficult but the increase in absolute accuracy of $\Delta r/r_b$ is worth it. (See, for example, fig. 6, ref. 1, which shows the surface recession profiles within and without a turbulence wedge.) Displacement error along the axis is minimized by positioning the images so that the computed mass loss from the average surface recession values matches the actual mass loss measured by weighing. This is done with the relation:

$$\frac{\Delta m}{m_o} = 6\Sigma\left(\frac{x}{x_b} - \frac{\Delta r}{2r_b}\right)\frac{\Delta r}{r_b}\frac{\Delta x}{x_b}$$

An earlier procedure, (ref. 1) that of matching the images along the model base plane, gave incorrect total mass losses. This is thought due to optical distortion resulting from diffraction of collimated light along the planar surface of the model base.

In addition to the quantitative data from the profiles, considerable information has been gained from microscopic examination of the ablated surfaces. This material was discussed quite extensively in references 1-4 so the discussion will not be repeated here.

RESULTS AND DISCUSSION

Total Mass Loss

The flight conditions and mass loss data for the Delrin 30° and 50° cones are listed in table I. A comparison of the observed mass losses with theory is shown in figure 3. Plotted as a function of the launch velocity is the measured mass loss normalized by the predicted turbulent mass loss. Both the laminar and turbulent theoretical mass loss, as well as local recession curves to be shown later, were calculated for sharp cones in the manner described in reference 2. These calculations take into account the deceleration of the model as well as the blockage of heat transfer by the ablation process.

A comparison of figures 3(a) and (b) indicates that the 30° cone data show predominately laminar flow, in contrast to the extensive turbulent flow experienced by the 50° cones. Mass loss data previously reported in reference 2, was interpreted as showing that similar 30° Delrin cones experienced extensive turbulent flow in the same velocity range. Those models, however, invariably had a damaged tip at launch. This damage is now thought to be responsible for the large extent of turbulent flow. Models that had obvious tip damage are not included here.

The numbers adjacent to some symbols give the percentage of nose radius to base radius for the model prior to launch. The results indicate that tip rounding prior to launch did not affect the results in any significant manner. However, some tip rounding naturally occurs during the flight, so that all the models perhaps should be considered as having rounded tips. The tip rounding incurred during flight due to ablation appears to make the prelaunch rounding, to the extent done, rather ineffective. Listed in table I are measurements showing the degree of tip radius increase during flight.

Although, as noted above, the 50° cone data show predominately turbulent boundary layer flow and the 30° cone data show predominately laminar boundary layer flow, it should not be inferred that the boundary layers were totally turbulent or

laminar. It is difficult, however, to estimate the Reynolds number of transition from these total mass loss data. More direct measurement of transition Reynolds numbers can be made from the surface recession results, as will be shown next.

Surface Recession

Surface recession measurement for the Delrin 30° cones are shown in figures 4 and 5. Surface recession is plotted against the boundary layer edge Reynolds number (based on edge conditions at launch and slant length of the cone). The local recession near the nose is in close agreement with that predicted by laminar theory. Although departure from the laminar mass loss curve occurs at Reynolds numbers as low as 1 to 2 million there still appears to be significant laminar flow even at Reynolds numbers to 14 million (see fig. 5(b)). This raises the question as to just how to interpret these data that, of course, represent ablation with variation of Reynolds number during the model's decelerating flight. If transition were fixed at some body position we would expect the recession curve to be similar to the well known laminar to turbulent (i.e., transition) heating curve. The length of this change from fully laminar to fully turbulent is approximately equal to the length of the preceding laminar flow. Even if transition occurs at a constant Reynolds number of transition, for example 1 million, and the transition region is of the same length as the laminar run the rear portions of these models would exhibit fully turbulent recession because most of the mass loss occurs at high speeds before the Reynolds number changes. As example, predicted recession curves for these two alternatives are shown in figure 4(c). Neither case is close to the measured results.

One possible interpretation is that transition is occurring at different transition Reynolds numbers on different rays. The results, then, can be interpreted in terms of the percentage of the circumference that is laminar at the launch Reynolds number. This is not the only possible interpretation of the results but it is the only one that does not require a rather complicated dependence of transition on flight conditions.

This simple view and very likely correct interpretation of the data suggests that at Reynolds numbers less than 1 million the flow is 100% laminar. At a Reynolds number of 5 million the flow is 20-30% turbulent; the exact amount depends on speed and pressure. Even at Reynolds numbers as high as 14 million only 60% of the boundary layer flow is

turbulent. These numbers, when compared with other free flight results on nonablating bodies (refs. 5 and 6), would suggest that for this ablator the effect of ablation on transition is not pronounced and if anything may even promote longer laminar flows. The low value of transition Reynolds number of 1 million for the first appearance of some turbulent flow is probably associated with local roughness effects. The evidence of considerable laminar flow at a Reynolds number of 14 million, although not impossible to obtain on a nonablating model with these local flow conditions, (e.g., refs. 5 and 6), is difficult to obtain because of roughness effects. Delrin ablates in such a manner as to yield a very smooth surface, provided there are no material imperfections. This then may be the reason for the apparent good performance during the present tests.

One final point to make is that, as noted in the preceding section, "Total Mass Loss," an initial nose radius of a few percent does not appear to alter the present results, (cf. figs. 4(b) and 5(c).

The recession measurements for Delrin 50° cones are shown in figure 6, plotted in the same manner as the 30° cone data. Note the striking difference. The data supports an interpretation of body fixed transition to turbulent flow near the nose of the body, (evident also in fig. 3). With the exception of the high speed tests shown in figure 6(a), very good agreement with turbulent boundary layer theory is apparent. Only in figure 6(d) is there an appearance of the behavior noted for the 30° cone data. Even here we see that at Reynolds numbers greater than 3 million fully turbulent flow is experienced. The lower value of transition Reynolds number on the 50° cones is probably due in part to the lower local boundary layer edge Mach number (ref. 7) (for a 30° cone $M_e \approx 4.5$ and for a 50° cone $M_e \approx 1.8$). This large difference in transition Reynolds number does not appear to be due to ablation effects as the ablation rates for the two cone angles is similar, (typically within 10-20%).

From figure 6 we note that the lowest value of the transition Reynolds number is less than 1/2 million. In fact, for the higher speed data, values considerably less than 1/2 million are indicated—the initial recession curves are always substantially above the laminar flow theory. The reason for this is not clearly understood at present. The erratic behaviour (one high and two low) exhibited for the three tests at about 6 km/sec (fig. 6(a)) is not fully understood at this time, particularly for the two models with the

lower recession. However, these two models had relatively low mass losses as shown by the two lowest points in figure 3(b). Surface inspections of the model with the larger recession indicate possible spalling that may be caused by launch damage or by thermal stresses.

Figures 7 and 8 present some additional data for models made of Lexan and cellulose nitrate. The data for 30° and 50° Lexan cones, (fig. 7) are very similar to the data obtained for the Delrin models. This general agreement between these results and those for Delrin (i.e., similar recession curves for 30° and 50° cone angles) is not surprising since they both have similar ablation characteristics (ref. 2). The theoretical recession curves for Lexan appear to be low, particularly when compared to the turbulent results in figure 7(c). This makes the determination of the first appearance of transitional flow from the data in figures 7(a) and 7(b) questionable. However, if one shifts the theoretical laminar curves upward until the data and theory curve agree near the nose we find that the departure of the data from the theory occurs between a Reynolds number of 1/2 and 1 million on the 30° Lexan cones. This apparently lower value of Reynolds number at the beginning of transition for Lexan when compared to Delrin may be due to a slightly rougher surface.

Figure 8 shows a comparison of recession curves at nominally the same test conditions, cone angle, velocity, and pressure, for models made of Delrin, Lexan, and cellulose nitrate. Note the large change exhibited by cellulose nitrate compared to the other two materials. Although a recession theory for cellulose nitrate is not available due to lack of ablation parameters, the recession curve suggests that the flow at the cone base is fully turbulent at a Reynolds number of about 2 million. This adverse effect of cellulose nitrate on transition may be due to the much higher laminar mass loss rate evident in figure 8. It may also be associated with combustion in the boundary layer since cellulose nitrate is known to be flammable.

CONCLUDING REMARKS

From the foregoing material, it is believed that four conclusions can be drawn:

(1) Significant amounts of laminar flow are possible on cones of moderately large half angle (30°) under some ablation conditions at Reynolds numbers (based on boundary-layer edge conditions) to 14 million.

(2) These large laminar runs are comparable to the longest laminar runs observed on nonablating surfaces at similar conditions.

(3) Larger angle cones (50°) experience considerable reduction in the transition Reynolds number. This is thought to be associated with the reduced edge Mach number.

(4) Cellulose nitrate exhibits much lower transition Reynolds number than Delrin and Lexan. Whether this is due to changes in ablation rate or to combustion in the boundary layer is not known at the present time.

SYMBOLS

m	mass of cone
m_o	mass of cone at launch
p/p_o	ballistic-range static pressure, atm
r	cone radius
r_b	cone base radius
r_n	tip radius
R_e	maximum local Reynolds number based on boundary-layer edge properties at launch
$(R_{e_x})_o$	local Reynolds number at launch along the slant length of the model
V_o	launch velocity
x	cone slant length measured from original apex
x_b	total cone slant length
θ_c	cone half angle

subscripts

m	measured
L	laminar, theoretical
T	turbulent, theoretical

TABLE I. MASS LOSS AND TIP RADIUS MEASUREMENTS

Model no.	Model material	θ_c, deg	V_o, km/sec	p/p_o, atm	m/m_o, measured	r_n/r_b, %, prelaunch	r_n/r_b, %, recovered
CN-1	cellulose nitrate	30	5.43	0.50	0.133	0.4	7.8
CN-2	cellulose nitrate	30	5.34	0.45	0.122	0.5	7.3
D-28	Delrin	30	4.88	1.0	0.0280	0.8	—
D-35	Delrin	30	5.42	1.0	0.0333	0.4	4.3
D-38	Delrin	30	4.27	1.0	0.0222	0.1	4.7
D-39	Delrin	30	2.99	1.0	0.0100	0.1	2.3
D-41	Delrin	30	6.25	1.0	0.0796	—	—
D-57	Delrin	30	3.05	1.0	0.0150	0.1	2.5
D-62	Delrin	30	3.05	1.0	0.0124	0.4	—
D-68	Delrin	30	3.81	1.0	0.0280	0.1	2.9
D-69	Delrin	30	3.66	1.0	0.0126	0.3	2.9
D-74	Delrin	30	3.89	1.0	0.0240	0.1	3.3
D-79	Delrin	30	2.20	1.0	0.0031	0.8	2.1
D-94	Delrin	30	5.73	1.0	0.0342	0.5	4.7
D-112	Delrin	30	5.43	1.0	0.0376	0.8	—
D-113	Delrin	30	5.18	1.0	0.0422	—	—
D-114	Delrin	30	5.37	1.0	0.0348	0.1	5.1
D-116	Delrin	30	5.11	1.0	0.0469	3.7	6.3
D-118	Delrin	30	5.03	1.0	0.0243	0.8	3.7
D-122	Delrin	30	6.10	1.0	0.0421	0.8	4.7
D-124	Delrin	30	5.95	1.0	0.0469	0.8	4.7
D-127	Delrin	30	5.49	1.0	0.0399	6.6	7.8
D-129	Delrin	30	5.73	1.0	0.0581	8.6	9.4
D-132	Delrin	30	6.10	1.0	0.0537	7.0	9.0
D-135	Delrin	30	5.03	1.0	0.0428	6.3	8.2
D-136	Delrin	30	5.19	0.59	0.0302	0.5	5.9
D-137	Delrin	30	5.95	0.50	0.0469	0.8	7.0
D-139	Delrin	30	5.49	0.47	0.0345	0.4	5.9

TABLE I. MASS LOSS AND TIP RADIUS MEASUREMENTS (Continued)

Model no.	Model material	θ_c, deg	V_o, km/sec	p/p_o, atm	m/m_o, measured	r_n/r_b, %, prelaunch	r_n/r_b, %, recovered
D-142	Delrin	30	5.49	0.52	0.0462	0.6	5.9
D-143	Delrin	30	5.12	0.56	0.0365	0.1	4.9
D-144	Delrin	30	5.03	0.60	0.0413	0.8	—
D-145	Delrin	30	5.34	0.51	0.0362	0.6	5.8
D-147	Delrin	30	5.49	0.45	0.0367	0.4	7.4
D-149	Delrin	30	5.18	0.43	0.0311	1.2	—
D-162	Delrin	30	5.80	2.72	0.0386	0.4	2.9
L-117	Lexan	30	6.31	0.40	0.0394	1.4	5.8
L-119	Lexan	30	5.49	0.50	0.0386	1.0	4.7
L-120	Lexan	30	5.34	0.55	0.0433	1.0	7.2
L-121	Lexan	30	5.40	0.45	0.0368	0.8	6.6
*DDC-3	Delrin	50	4.27	4.06	0.0921	0.9	4.7
DDC-5	Delrin	50	5.49	3.03	0.1743	1.7	6.3
DDC-6	Delrin	50	5.95	3.09	0.1300	0.8	5.7
DDC-7	Delrin	50	4.88	3.09	0.1288	1.2	5.3
DDC-9	Delrin	50	5.95	3.13	0.2133	1.0	5.6
DDC-10	Delrin	50	4.27	3.12	0.0834	1.3	5.0
LDC-1	Delrin	50	6.10	3.12	0.1304	1.6	6.6
LDC-4	Delrin	50	4.27	3.10	0.0961	4.7	6.3
LDC-6	Delrin	50	5.70	3.09	0.1568	0.8	5.2
LDC-7	Delrin	50	5.12	3.10	0.1190	0.7	3.3
LLC-2	Lexan	50	4.12	3.14	0.0945	1.2	4.5

*First letter denotes the model material, second letter the cylinder material, D = Delrin, L = Lexan (see fig. 1).

REFERENCES

1. Thomas N. Canning, Michael E. Tauber, and Max E. Wilkins, Review of Recent Ballistic Range Boundary-Layer Transition Work on Ablating Bodies at Ames. Boundary Layer Transition Study Group Meeting, Vol. III, W. D. McCauley, ed., Aerospace Rep. No. TR-0158 (S3816-63) - 1, III, Aerospace Corp., San Bernardino, Calif. (August 1967). (Also available as Air Force Report No. BSD-TR-67-213, Vol. III.)

2. Max E. Wilkins and Michael E. Tauber, Boundary-Layer Transition on Ablating Cones at Speeds Up to 7 Km/Sec, AIAA J., pp. 1344-1348 (August 1966).

3. Max E. Wilkins, Evidence of Surface Waves and Spreading of Turbulence on Ablating Models, AIAA J., Vol. 3, pp. 1963-1966 (1965).

4. Thomas N. Canning, Max E. Wilkins, and Michael E. Tauber, Boundary-Layer Phenomena Observed on the Ablated Surfaces of Cones Recovered After Flights at Speeds Up to 7 Km/Sec. AGARD Specialists' Meeting on Fluid Physics of Hypersonic Wakes, Fort Collins, Colorado, May 10-12, 1967. AGARD Conference Proceedings No. 19.

5. James R. Jedlicka, Max E. Wilkins, and Alvin Seiff, Experimental Determination of Boundary-Layer Transition on a Body of Revolution at M = 3.5. NACA TN 3342, 1954.

6. Carlton S. James, Boundary-Layer Transition on Hollow Cylinders in Supersonic Free Flight as Affected by Mach Number and a Screwthread Type of Surface Roughness. NASA Memo 1-20-59A, 1959.

7. A. L. Nagel, Compressible Boundary Layer Stability by Time-Integration of the Navier-Stokes Equations, and an Extension of Emmons' Transition Theory to Hypersonic Flow. (Same as ref. 1 above except Vol. II, instead of III.)

FREE FLIGHT DETERMINATION OF BOUNDARY LAYER TRANSITION ON SMALL SCALE CONES IN THE PRESENCE OF SURFACE ABLATION

TABLE

FIGURES

(a) V_o = 5.03 km/sec

(b) V_o = 5.37 km/sec

(c) V_o = 5.95 km/sec

5 Surface recession (averaged around periphery) on Delrin cones, $\theta_c = 30°$

(a) V_o = 5.19 km/sec, p/p_c = 0.591

(b) V_o = 5.80 km/sec, p/p_o = 2.72

(c) V_o = 5.49 km/sec, p/p_o = 1.0, r_n/r_b = 0.07

6 Surface recession (averaged around periphery) on Delrin cones, $\theta_c = 50°$

(a) V_o = 5.94 km/sec (DDC-6 & DDC-9), V_o = 6.10 km/sec (LDC-1), p/p_o = 3.1

(b) V_o = 5.49 km/sec (DDC-5), V_o = 5.70 km/sec (LDC-6), p/p_o = 3.1

(c) V_o = 4.88 km/sec, p/p_o = 3.1

(d) V_o = 4.27 km/sec, p/p_o = 3.1

(e) V_o = 4.27 km/sec, p/p_o = 4.1

7 Surface recession (averaged around periphery) on Lexan cones

(a) $\theta_c = 30°$

(b) $\theta_c = 30°$, V_o = 6.31 km/sec, p/p_o = 0.399

(c) $\theta_c = 50°$, V_o = 4.12 km/sec, p/p_o = 3.14

8 Surface recession (averaged around periphery) on cones of different materials, $\theta_c = 30°$

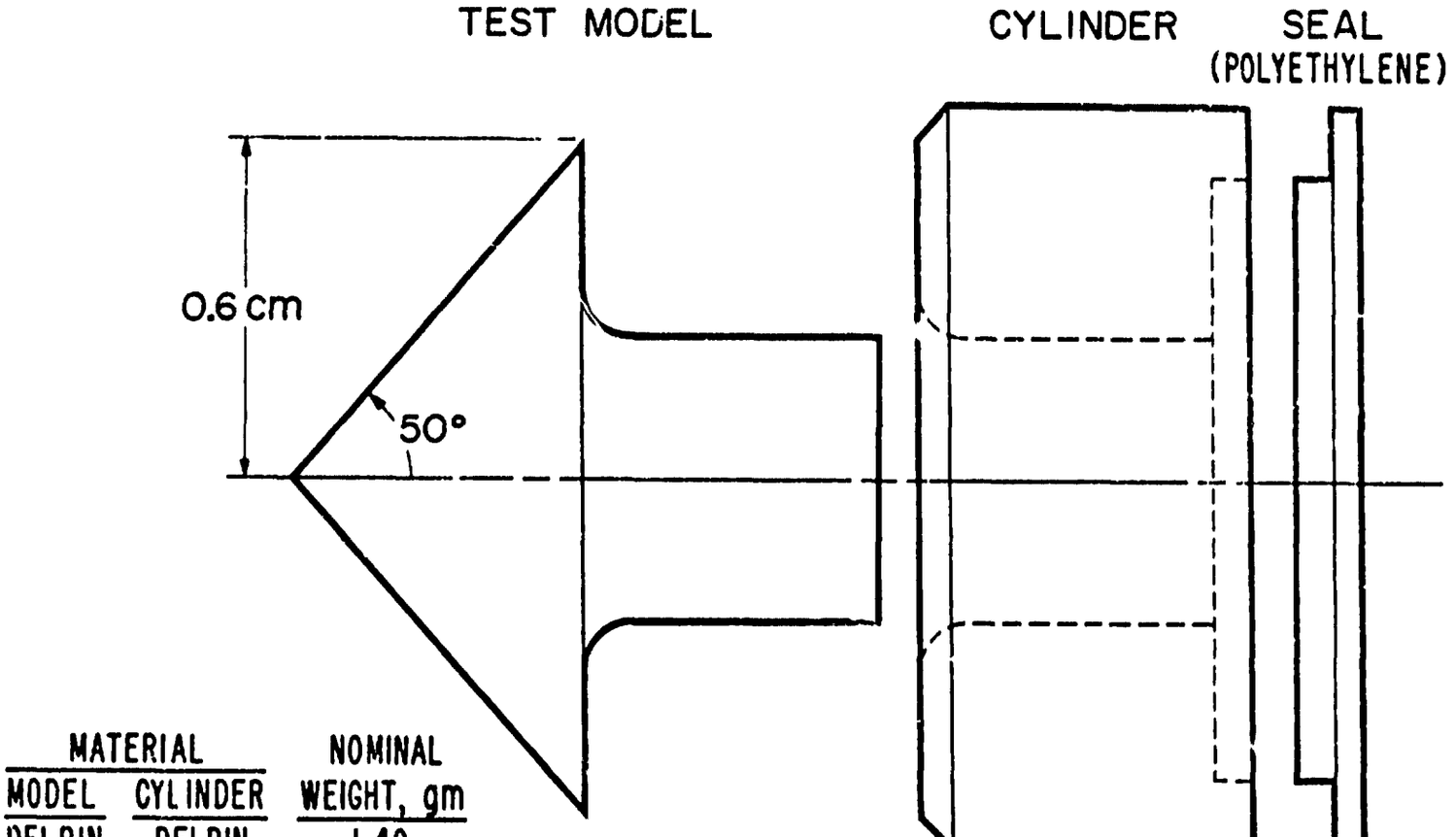

MATERIAL		NOMINAL
MODEL	CYLINDER	WEIGHT, gm
DELRIN	DELRIN	1.40
DELRIN	LEXAN	1.28
LEXAN	LEXAN	1.21

Figure 1. Model configuration, $\theta_c = 50°$

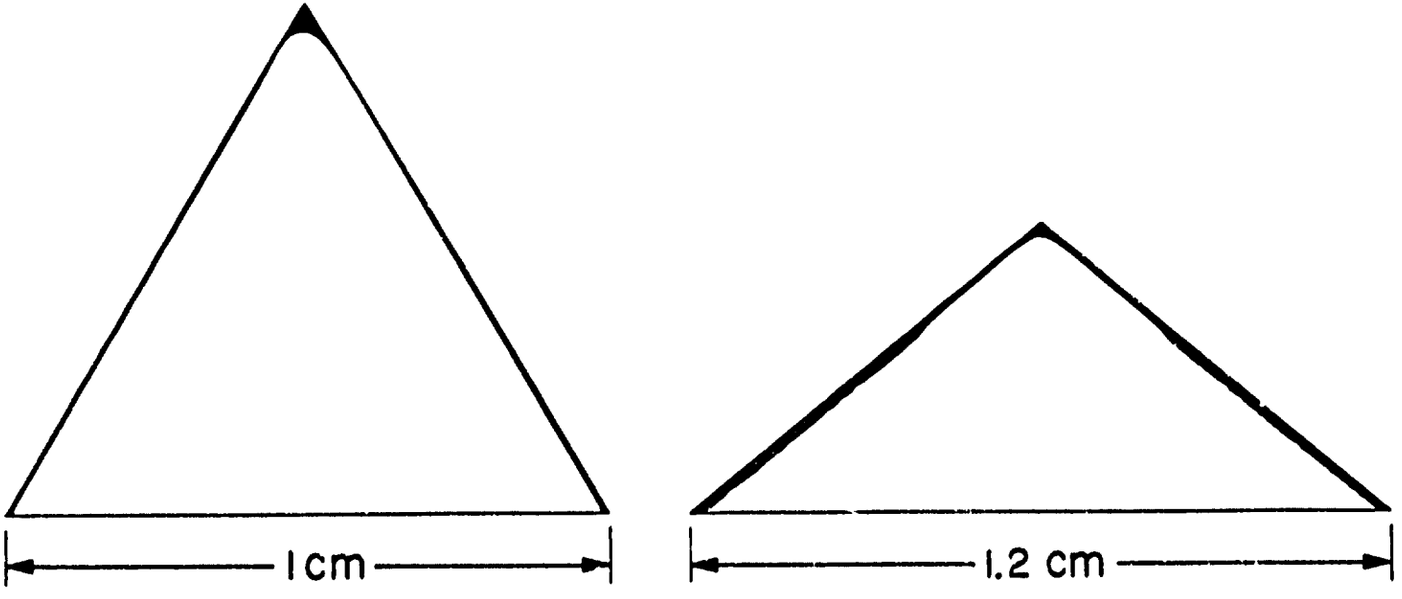

(a) $\theta_c = 30°$, $V_o = 6.4$ km/sec

(b) $\theta_c = 50°$, $V_o = 4.9$ km/sec

Figure 2. Typical profiles of Delrin models before launch and after recovery.

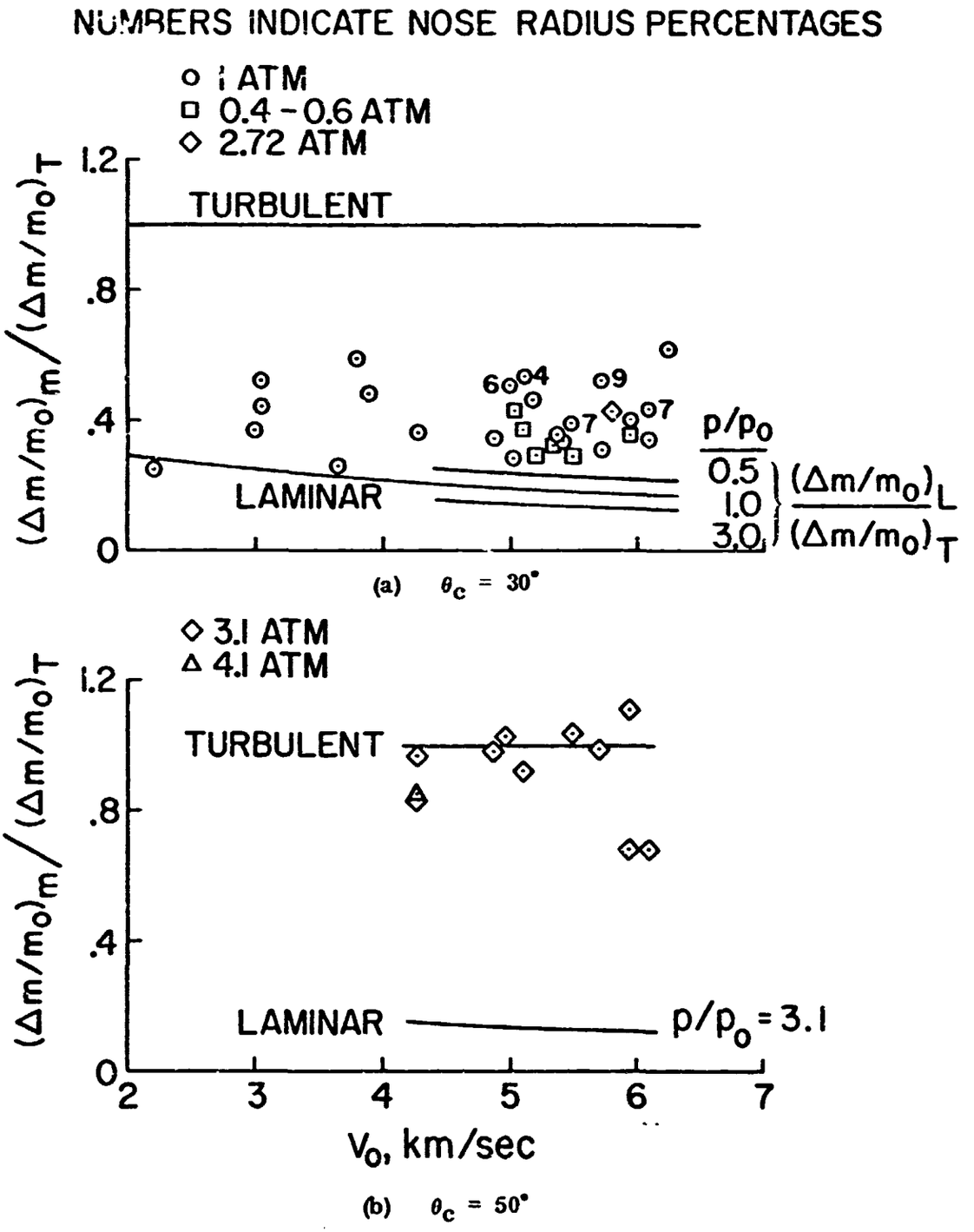

Figure 3. Total mass loss for Delrin cones

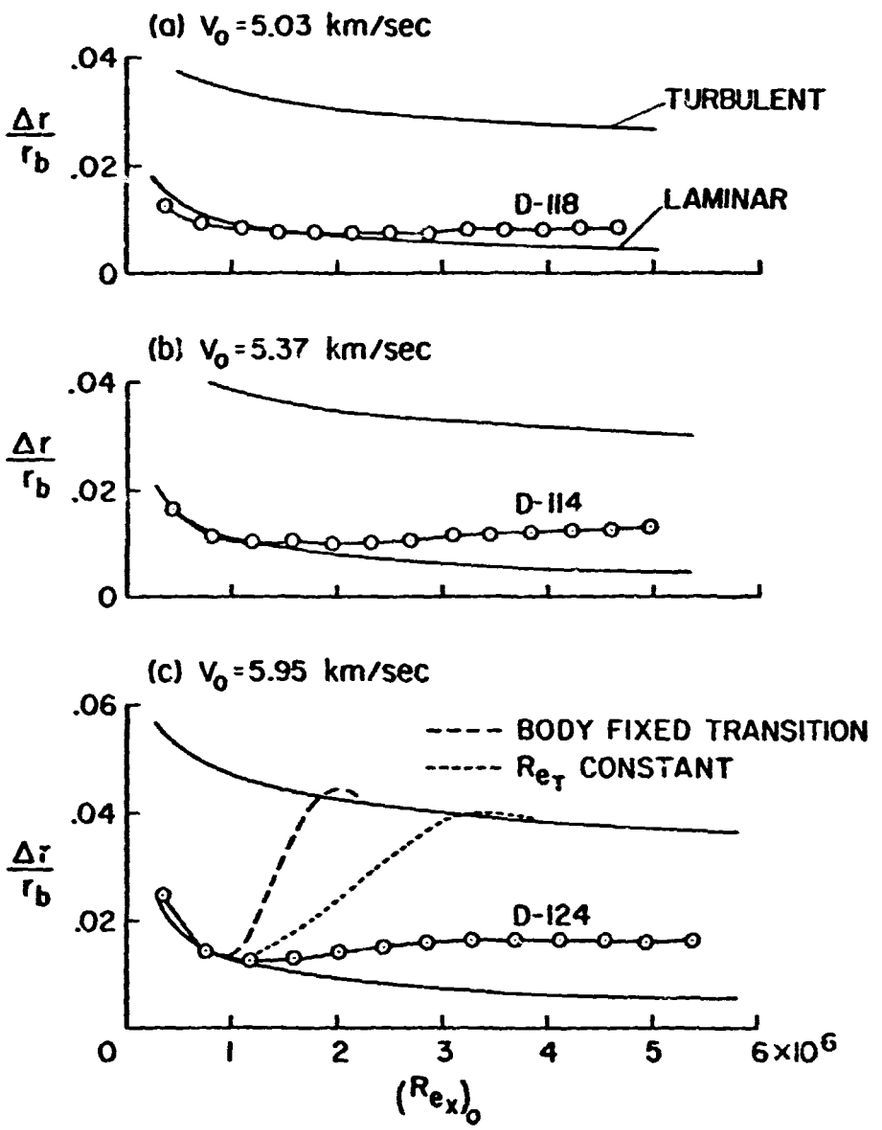

Figure 4. Surface recession (averaged around periphery) on Delrin cones, $\theta_c = 30°$, $p/p_0 = 1$

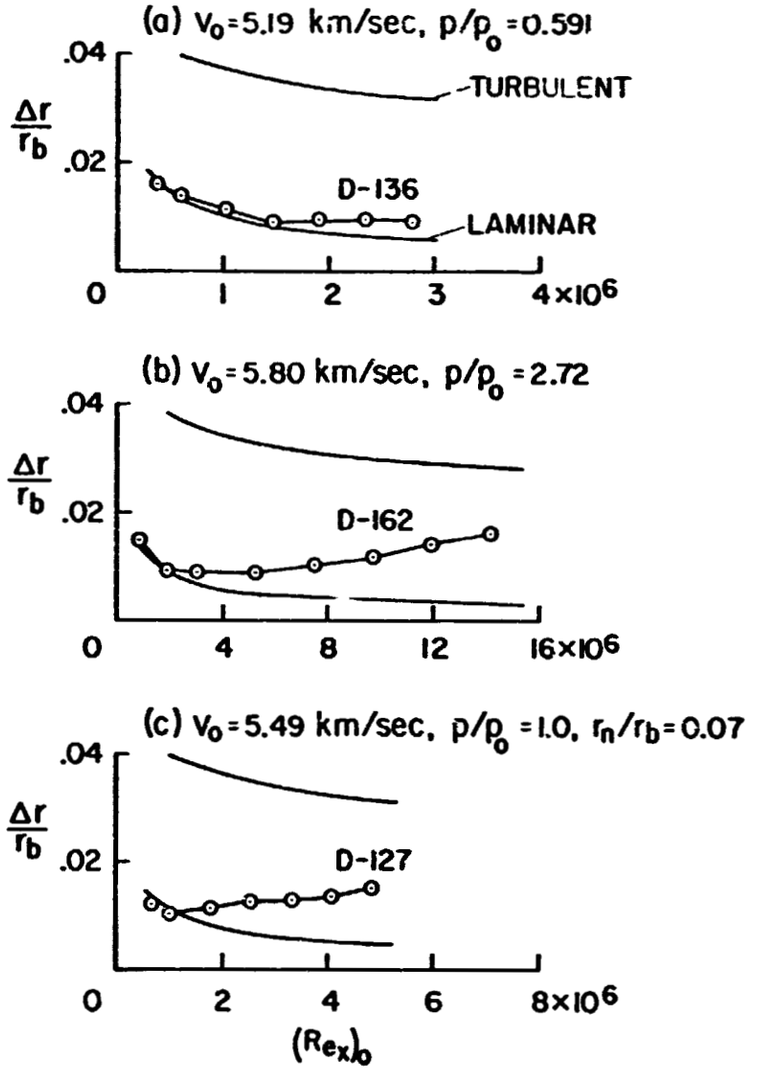

Figure 5. Surface recession (averaged around periphery) on Delrin cones, $\theta_c = 30°$

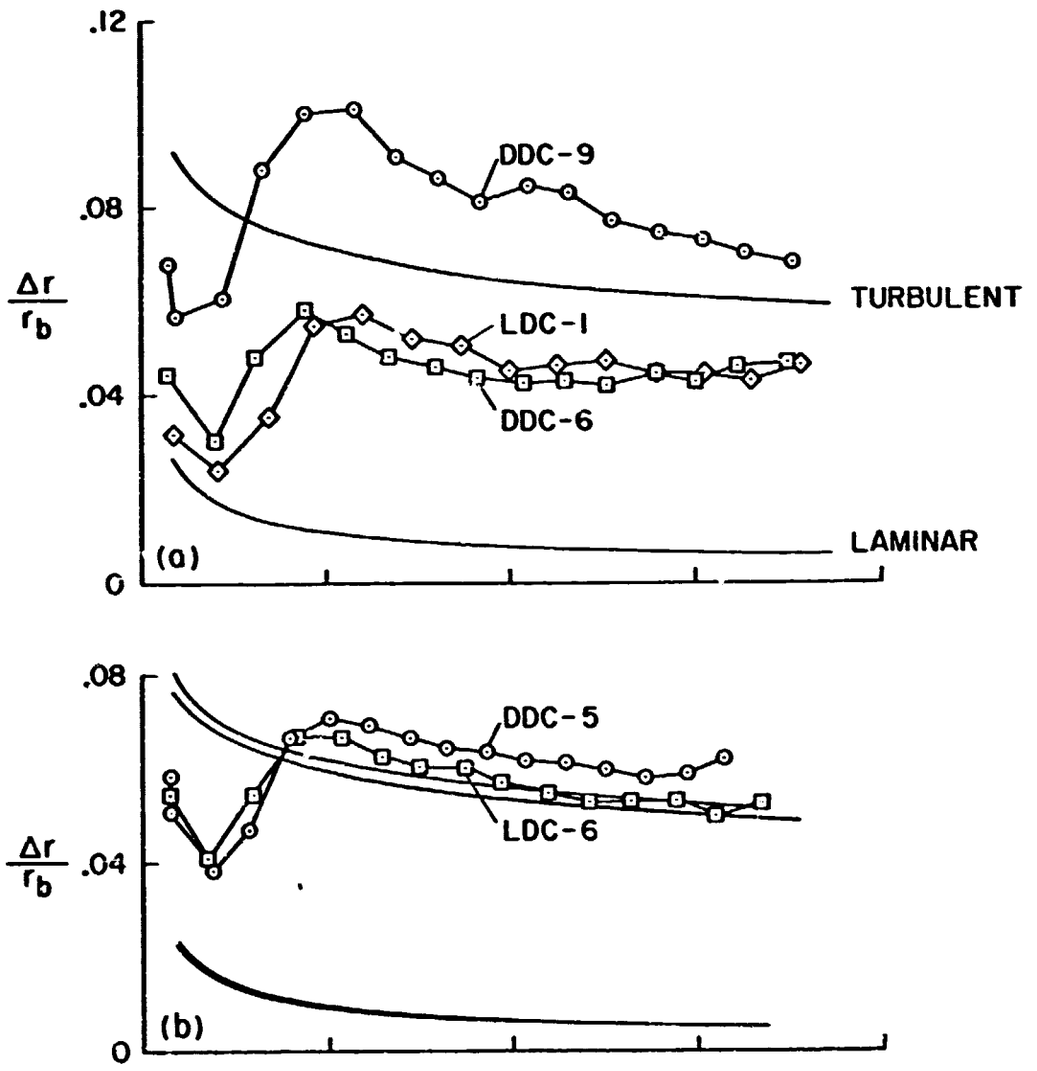

(a) V_o = 5.94 km/sec (DDC-6 & DDC-9), V_o = 6.10 km/sec (LDC-1), p/p_o = 3.1

(b) V_o = 5.49 km/sec (DDC-5), V_o = 5.70 km/sec (LDC-6), p/p_o = 3.1

Figure 6. Surface recession (averaged around periphery) on Delrin cones, θ_c = 50°

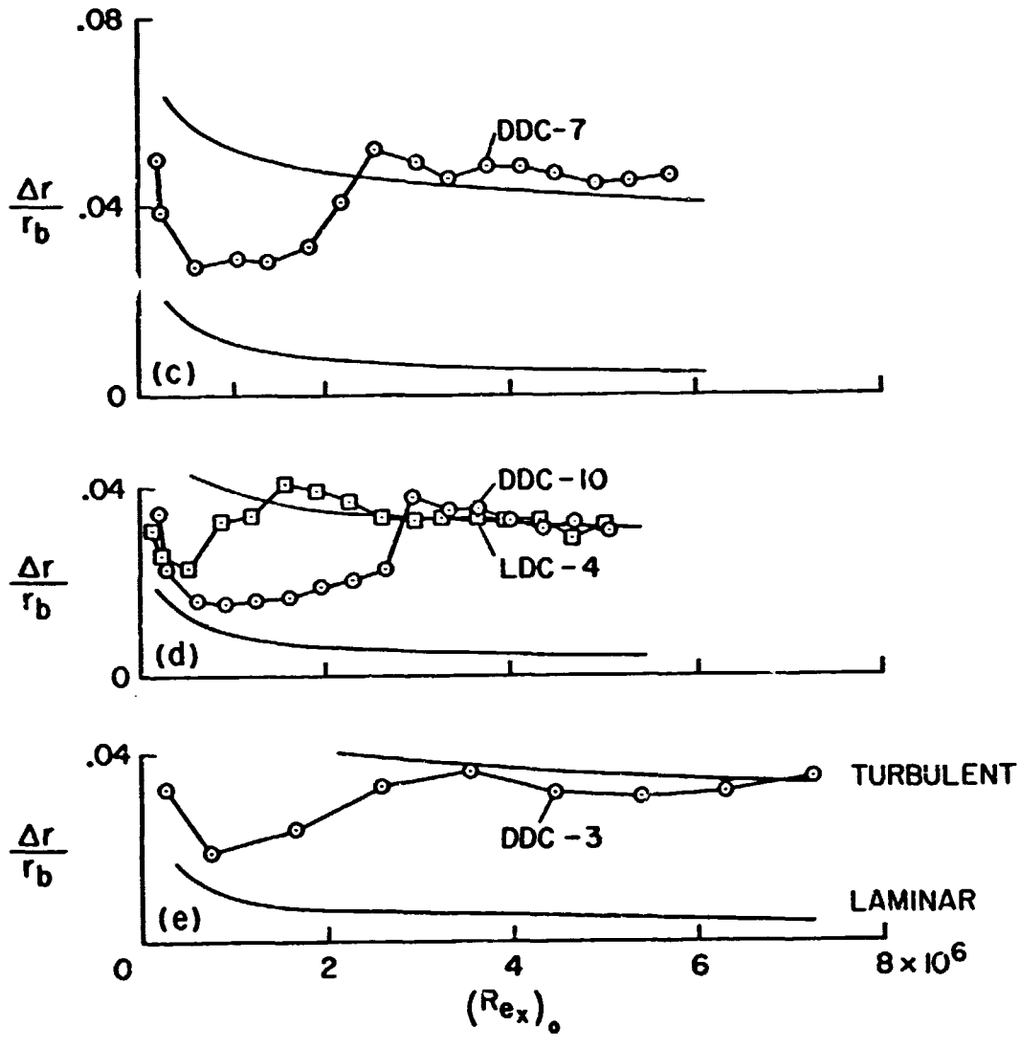

(c) V_o = 4.88 km/sec, p/p_o = 3.1

(d) V_o = 4.27 km/sec, p/p_o = 3.1

(e) V_o = 4.27 km/sec, p/p_o = 4.1

Figure 6 Concluded.

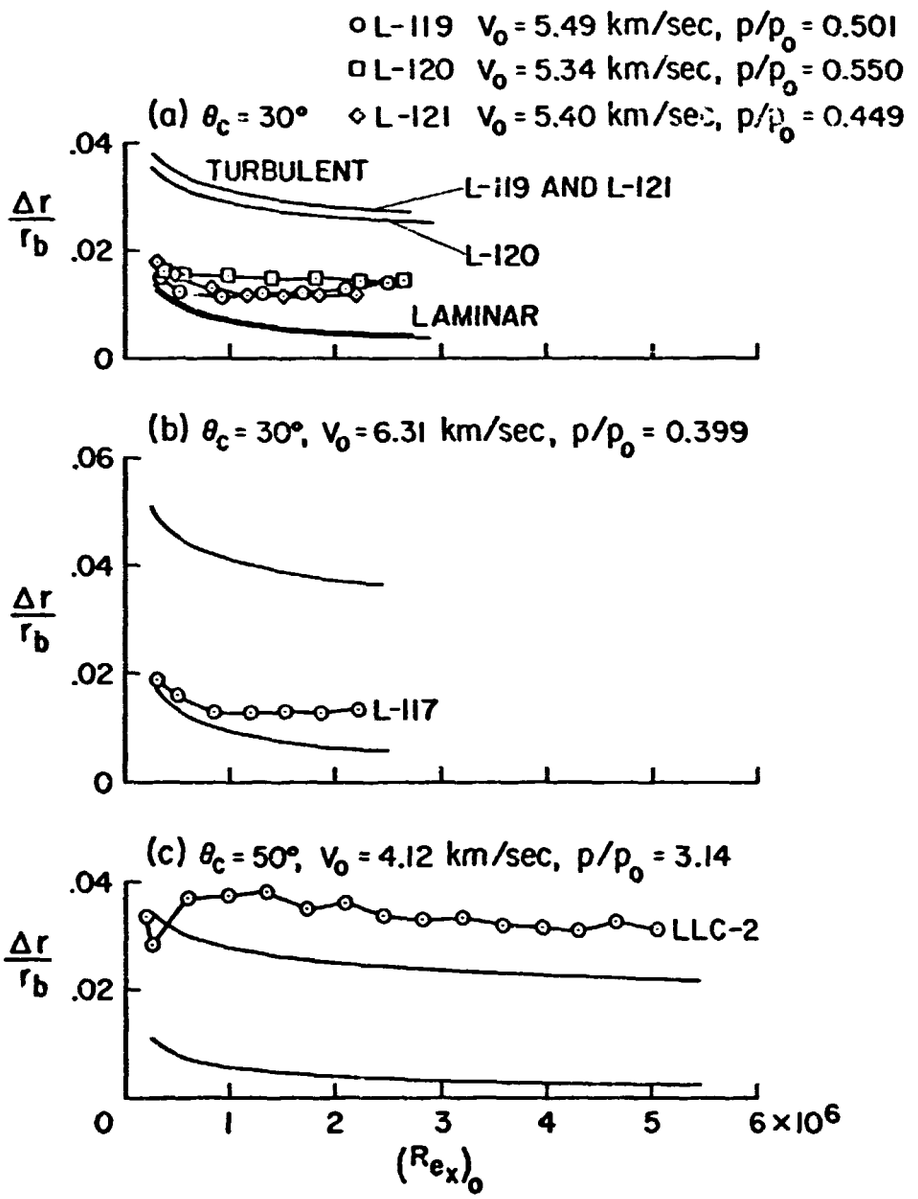

Figure 7. Surface recession (averaged around periphery) on Lexan cones

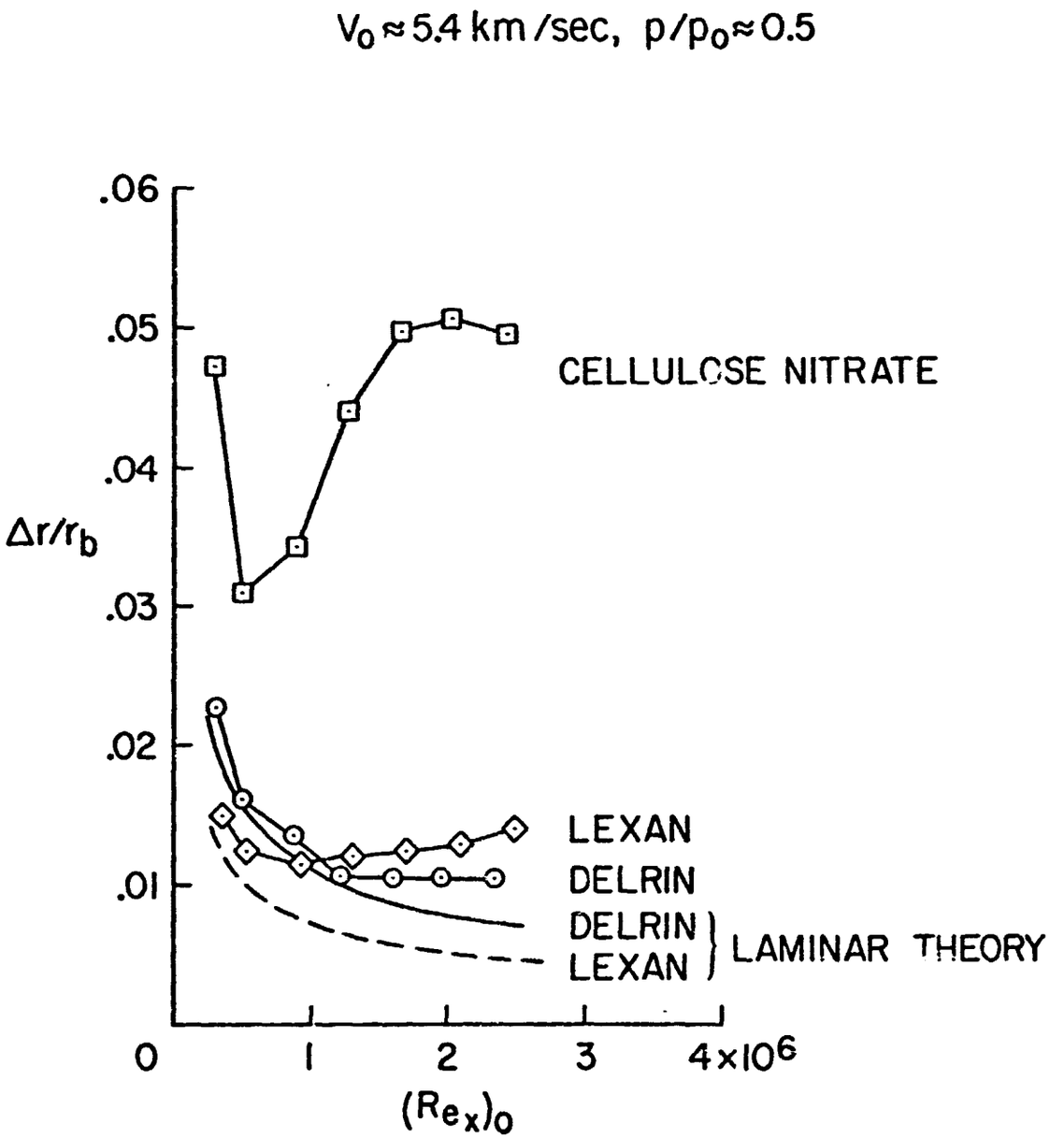

Figure 8. Surface recession (averaged around periphery) on cones of different materials, $\theta_c = 30°$